Research Paper   Open Access

Two-Dimensional model of a Delugeable Flat Bare Tube Air-Cooled Steam Condenser Bundle

Angula Ester[1*]

[1]Department of Mechanical and Industrial Engineering,
Faculty of Engineering and Information Technology, University of Namibia
Eng. José Eduardo dos Santos Campus, P.O. Box 3624, Ongwediva, Namibia
*Corresponding Author: Angula Ester

ABSTRACT: *In this paper, a two-dimensional model was developed for the numerical evaluation of the thermal performance of a delugeable flat tube bundle to be incorporated in the second stage of an induced draft hybrid (dry/wet) dephlegmator (HDWD) of a direct air-cooled steam condenser (ACSC). The heat and mass transfer analogy method of analysis was employed during the evaluation, and the governing differential equations were discretised into algebraic equations using linear upwind differencing scheme. The two-dimensional model's accuracy was validated through a comparison of its solutions to one dimensional model solutions presented in Angula (2018), where the heat and mass transfer analogy, Merkel, and Poppe approaches were usedfor the analytical evaluation of the thermal performance of the same tube bundle. Satisfactory correlation between the one and two-dimensional results was reached. However, the heat transfer rates yielded from one-dimensional model were found to be slightly higher than that obtained from two-dimensional model with differences of 1.98%, 8.23%, and 10.79% for heat and mass transfer analogy, Merkel, and Poppe methods, respectively. The difference in air-side pressure drop obtained by all the methods was found to be insignificant. Furthermore, the identification of best configuration of a delugeable flat tube bundlefor the second stage of induced draft HDWD wascarried out, through the comparison study of its performance to that of round tube bundle. The performance of the round tube bundle was found to be 1.95 times, and 1.43 times of that of flat tube bundle, when both bundles operate as an evaporative and dry air-cooled condenser, respectively.*

KEYWORDS: *Flat, Bare, Delugeable, Dephlegmator, Heat and Mass transfer, Wet, Dry, Two-dimensional*

Date of Submission: 19-05-2018   Date of acceptance: 04-06-2018

I   INTRODUCTION

Application of ACSC and dry cooling towers to reject heat into the environment in dry-cooled power plants incorporating steam turbines, became widely. This is due to water shortage, as well as water restriction that have been imposed. During the hot periods, ACSC experience performance penalties, which badly affect the output power of the steam turbine. Therefore, the performance improvement of ACSC is essential. The HDWD as an ACSC's enhancement technique, is found to be cost effective and it uses around 20% less water than for the pre-cooling technology [1]. The HDWD is to replace a dry convectional dephlegmator in each Street of an ACSC. The role of the dephlegmator is to eject the non-condensable gases and condensing the excess steam, which results in good stability and acceleration of the steam flow in the primary condenser units. Therefore, it is meaningful to improve the dephlegmator performance, since this will directly lead to the overall performance improvement of the power plant.

For that reason, this paper aims to analyse the thermal performance of a delugeable flat bare tube bundle to be incorporated in the second stage of an induced

 draft HDWD of a direct ACSC, by employing the two-dimensional numerical model. The HDWD can be forced or induced draft as shown in Figure 1 and has two stages connected in series and combined in one condenser unit. The first stage has inclined finned tubes and second stage has horizontal smooth tubes. The second stage operates in the dry mode as an Air-Cooled Condenser (ACC) during cold or off-peak periods, and in the wet mode as evaporatively cooled condenser during hot and peak periods.

During the wet operating mode, the deluge water is sprayed over the surface of the second stage tubes, which then collected in troughs under the tube bundle, while the water droplets blown up by the air are trapped by the drift eliminator above the tube bundle. The corrosion and fouling risk that may rise during the wet operating mode, are mitigated by using the smooth bare tubes in the second stage.

a) **Forced HDWD**
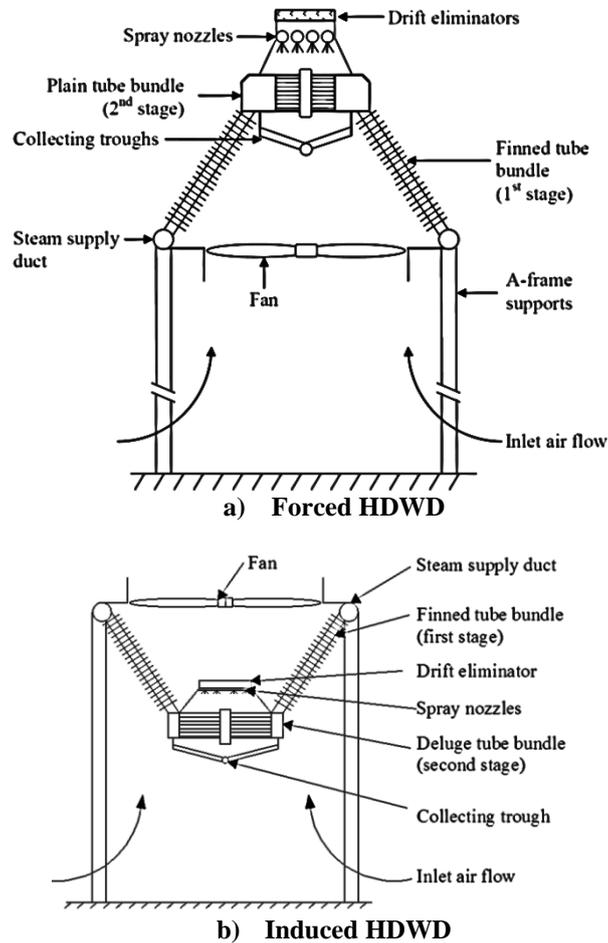
b) **Induced HDWD**
Figure 1: Schematic diagram of the HDWD[2]

Analysis of the thermal performance characteristics of the evaporatively cooled heat exchangers started far back with researchers such as Parker & Treybal[3] and Mizushina, et al.[4], who conducted the analytical and numerical analysis of the evaporative cooler characteristics by employing Merkel[5] model, in which the evaporation of the deluge water was neglected, the Lewis factor taken to be equal to unity, and the enthalpy of the saturated air was assumed. A comparative analysis of the round plain and finned tube bundle of an evaporative heat exchanger was carried out by Hasan & Siren [6]. The plain tube bundle showed higher mass transfer coefficient than finned. However, due to the large surface area of the finned tube bundle, the heat transfer rate for the finned tube bundle found to be higher.

The performance evaluation of the finned round, plain round, louver fin flat and oval tube bundle of an evaporative heat exchanger, have been performed by several researchers such as Yang & Clark[7] and Leidenforst & Korenic [8], Jahangeer, et al.[9], Zhang , et al.[10] and Hasan & Siren [11]and Zheng , et al.[12]. Numerous studies have been carried out in an attempt to identify a configuration of the HDWD second stage's tube bundle that provides higher performance. Most of the researchers focused in delugeable round tube bundle analysis. Heyns[13] investigated a delugeable bundle performance of 38 mm diameter round tubes for the forced draft HDWD, while Owen[14], Anderson[15] and Graaff[16]analysed 19 mm diameter round tube bundle for the induced draft HDWD.

Heyns[13]'s tube bundle was then incorporated in Heyns and Kröger [1] study in which the output power of the steam turbine cooled by Air-cooled Condenser (ACC) incorporating the HDWD, ACC with pre-cooling of inlet air, and over-sized ACC by 33% were compared. The water consumption of the HDWD was found to be around 20% less water than for the pre-cooling technology, and the cost difference between the

HDWD and the convectional dephlegmator is small. Owen [14] compared the HDWD and convectional dephlegmator performance, on a component level (for the whole dephlegmator) and on a system level (for the whole ACC). On a component level, the performance of HDWD was found to be two to three times that of the convectional dephlegmator when operate in wet mode, while on a system level, the ACC's heat transfer rate with five primary condensers and one HDWD was 15% -30% higher than for a similar ACC with convectional dephlegmator. Anderson (2014)'s experimental data and tube bundle were employed in Reuter and Anderson[17] and Graaff[16] works respectively. Based on Anderson [15]'s experimental data, Anderson and Reuter [17] derived the correlations of mass transfer, heat transfer and air-side pressure loss coefficient for the round bare tube bundle under wet and dry operation conditions. All correlations were found to be functions of the air mass velocity, the deluge water flow rate and mean deluge water temperature. Graaff [16] investigated the performance of a hybrid (dry/wet) cooling system (HDWCS) by using the correlations of Anderson (2014) and Mizushina et al. [4]. At different air relative humidity and an ambient dry bulb temperature of 32 ℃, the HDWCS' performance was found to be between 35 % and 140 % relative to a conventional cooling system. The performance a delugeable flat bare tube bundle of 1 m height and 3.86 and 6.86 mm inside and outside width respectively, for the induced draft HDWD was investigated analytical in Angula[2], the model was based on Merkel[5], Poppe[18], and heat and mass transfer analogy. The tube bundle was found to deliver higher performance during wet operating conditions than during dry operating conditions.

As stated above, in most of the studies, round tube bundles were considered, except in Angula[2]where one-dimensional analytical analysis of flat tube bundle was conducted. The literatures lack information on numerical performance analysis of the bare flat tube bundle operating under deluging conditions. Therefore, this paper evaluates numerically the thermal performance of the bare flat tube bundle for an induced draft HDWD of an ACSC.

II   MATERIALS AND METHODS

2.1.   Two-dimensional model

The thermal performance of a delugeable flat tube bundle was evaluated by means of a two-dimensional numerical model. A schematic of two tubes in a delugeable flat tube bundle for the ACSC is shown in Figure 2.
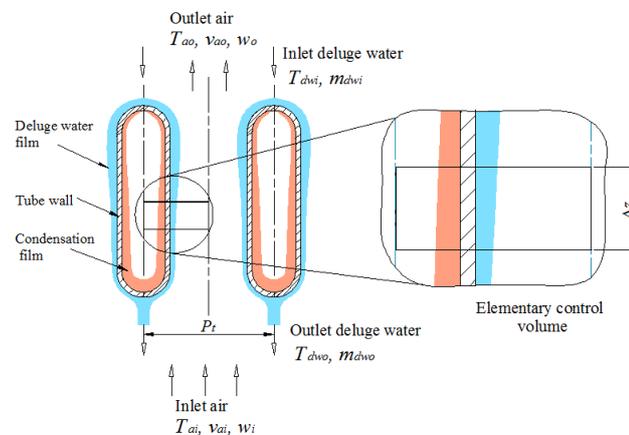
Figure 2: Schematic diagram of two adjacent tubes in a delugeable flat bare tube bundle[2]

An elementary control volume was drawn from the centreline of the tube to the symmetry line between the two adjacent tubes as indicated in Figure 2. The two-dimensional elementary control volume of the delugeable horizontal bare flat tube bundle is shown in Figure 3. The counter-current flow configuration of air and water over the surface of the tubes was considered. The steam flows inside the tubes in the *x*-direction, and the condensate drains in the negative *z*-direction. The steam is condensed by the deluge water and cooling air flow over the tubes. A condensation film is formed inside the tubes and runs down the tube wall along the height due to gravity. The recirculating deluge water was sprayed over the tube surface in the negative *z*-direction, while the inlet air was drawn upward from the bottom of the tubes in the *z*-direction. The heat is transferred from the condensed steam through the condensation film, tube wall, deluge water film, and finally crosses the air-water interface to the air stream. Due to the direct contact of air and water at the air-water interface, the deluge water evaporates into the air stream.
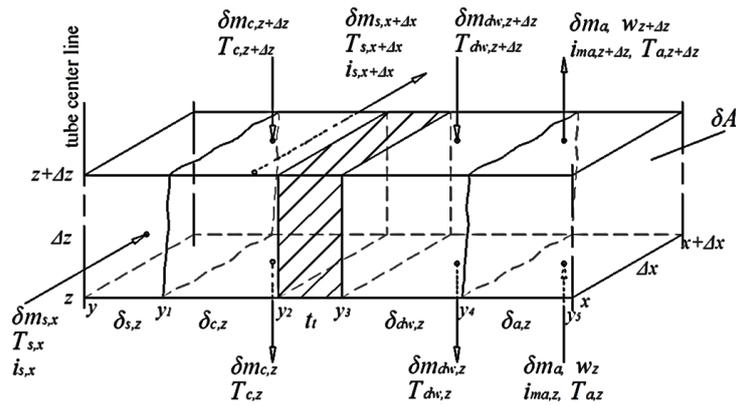
Figure 3: The two-dimensional elementary control volume of the delugeable horizontal bare flat tube bundle

The different y-values in Figure 3 can be written as:

$$y_1 = y + \delta_{s,z} \tag{1}$$
$$y_2 = y_1 + \delta_{c,z} \tag{2}$$
$$y_3 = y_2 + t_t \tag{3}$$
$$y_4 = y_3 + \delta_{dw,z} \tag{4}$$
$$y_5 = y_4 + \delta_{a,z} \tag{5}$$

The two-dimensional approach provides more detailed information on the heat and mass transfer processes taking place in the tube bundle. Unlike one-dimensional analysis, two-dimensional analysis takes into account the heat transfer in both *z* and *y*-directions. The two-dimensional elementary control volume shown in Figure 3was divided into five elementary control volumes which are: steam-side, condensate-side, tube wall-side, deluge water-side and air-side, which are shown in Figures 4(a), 5, 7(a), 8 and 10, respectively. The two-dimensional model was developed from the principles of conservation of mass, energy and momentum.

2.1.1.   *Steam-side elementary control volume*
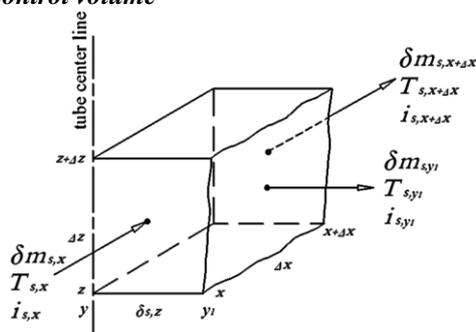
a)   **Elementary control volume**
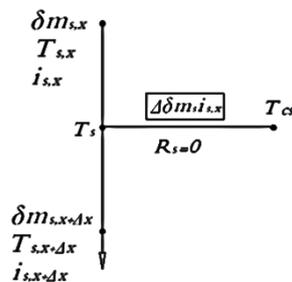
b)   **Thermal resistance diagram**

Figure 4: Steam-side elementary control volume and thermal resistance diagram

a)   The mass balance for the elementary control volume

$$\delta m_{s,x} = \delta m_{s,x+\Delta x} + \delta m_{s,y_1} \tag{6}$$

That can be simplified as

$$\Delta \delta m_{s,x} = \delta m_{s,y_1} \tag{7}$$

b)   The energy balance for the elementary control volume

$$\delta m_{s,x} i_{s,x} = \delta m_{s,x+\Delta x} i_{s,x+\Delta x} + \delta m_{s,y_1} i_{s,y_1} \tag{8}$$

Assume that $i_{s,x} = i_{s,x+\Delta x} = i_{s,y_1}$ then, Eq. (8) becomes

$$\Delta \delta m_{s,x} i_{s,x} = \delta m_{s,y_1} i_{s,y_1} \tag{9}$$

2.1.2.   Condensate-side elementary control volume
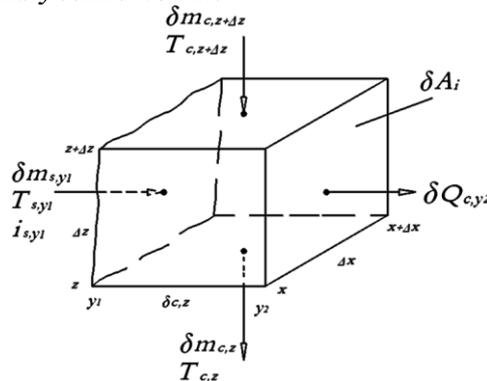
Figure 5: Condensate-side elementary control volume

a)   The mass balance for the elementary control volume

$$\delta m_{s,y_1} + \delta m_{c,z+\Delta z} = \delta m_{c,z} \tag{10}$$

That can be simplified as

$$\delta m_{s,y_1} = \Delta \delta m_{c,z} \tag{11}$$

b)   The energy balance for the elementary control volume

$$\delta m_{s,y_1} i_{s,y_1} + \delta m_{c,z+\Delta z} c_{pc} T_{c,z+\Delta z} = \delta m_{c,z} c_{pc} T_{c,z} + \delta Q_{c,y_2} \tag{12}$$

Substitute Eq. (9) into Eq. (12) and simplify

$$\delta Q_{c,y_2} = \Delta \delta m_{c,z}(i_{s,x} - c_{pc} T_{c,z+\Delta z}) + \delta m_{c,z} c_{pc} \Delta T_{c,z} \tag{13}$$
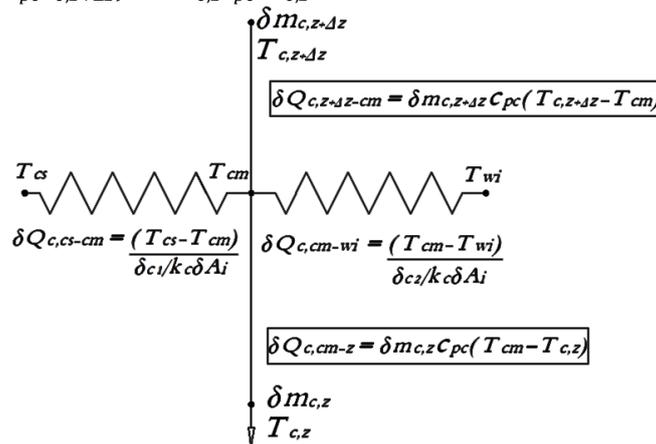
Figure 6: Condensate-side thermal resistance diagram

c)   The heat transfer balance for the thermal resistance diagram

$$\delta Q_{c,cs-cm} + \delta Q_{c,z+\Delta z-cm} = \delta Q_{c,cm-wi} + \delta Q_{c,cm-z} \tag{14}$$

d)   Coupling of the elementary control volume to thermal resistance diagram

$$\delta Q_{c,cs-cm} = \delta m_{s,y_1} i_{s,y_1} = \Delta \delta m_{c,z} i_{s,x} \tag{15}$$

$$\delta Q_{c,cm-wi} = \delta Q_{c,y_2} \tag{16}$$

From the momentum balance of the elementary control volume within the condensation film, the weighted mean temperature of the condensate in the condensation film is

$$T_{cm} = T_{cs} - \frac{3(T_{cs} - T_{wi})}{4} \tag{17}$$

2.1.3. Tube wall-side elementary control volume

a) Control volume

b) Thermal resistance diagram
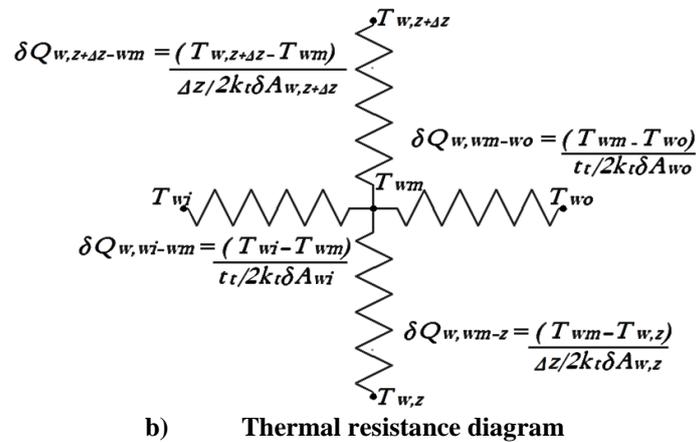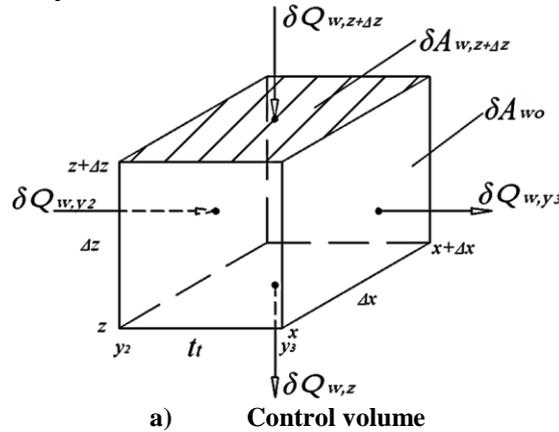
Figure 7: Tube wall-side elementary control volume and thermal resistance diagram

a) The heat transfer balance for the thermal resistance diagram

$$\delta Q_{w,wi-wm} + \delta Q_{w,z+\Delta z-wm} = \delta Q_{w,wm-wo} + \delta Q_{w,wm-z} \tag{18}$$

and

$$\delta A_{wi} = \delta A_{wo} \tag{19}$$
$$\delta A_{w,z} = \delta A_{w,z+\Delta z} \tag{20}$$

b) Coupling of the elementary control volume to thermal resistance diagram

$$\delta Q_{w,wi-wm} = \delta Q_{w,y_2} = \delta Q_{c,y_2} \tag{21}$$
$$\delta Q_{w,z+\Delta z-wm} = \delta Q_{w,z+\Delta z} \tag{22}$$
$$\delta Q_{w,wm-wo} = \delta Q_{w,y_3} \tag{23}$$
$$\delta Q_{w,wm-z} = \delta Q_{w,z} \tag{24}$$

2.1.4. Deluge water elementary control volume
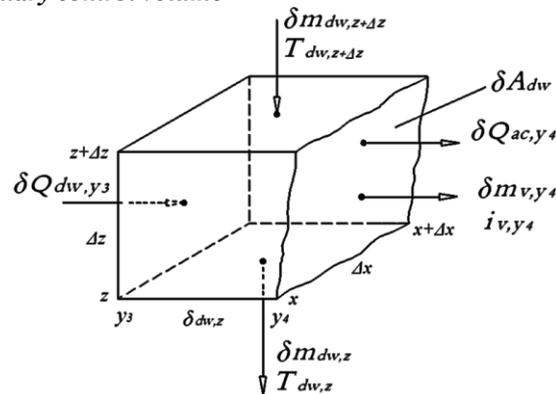
Figure 8: Deluge water-side elementary control volume

a) The water mass balance for the elementary control volume

$$\delta m_{dw,z+\Delta z} = \delta m_{dw,z} + \delta m_{v,y_4} \tag{25}$$

That can be simplified as

$$\Delta \delta m_{dw,z} = \delta m_{v,y_4} \tag{26}$$

b) The energy balance for the elementary control volume

$$\delta Q_{dw,y_3} + \delta m_{dw,z+\Delta z} c_{pdw} T_{dw,z+\Delta z} = \delta m_{dw,z} c_{pdw} T_{dw,z} + \delta Q_{ac,y_4} + \delta m_{v,y_4} i_{v,y_4} \tag{27}$$

Substitute Eq. (26) into Eq. (27) and simplify

$$\delta Q_{ac,y_4} = \Delta \delta m_{dw,z} (c_{pdw} T_{dw,z+\Delta z} - i_{v,y_4}) + \delta m_{dw,z} c_{pdw} \Delta T_{dw,z} + \delta Q_{dw,y_3} \tag{28}$$
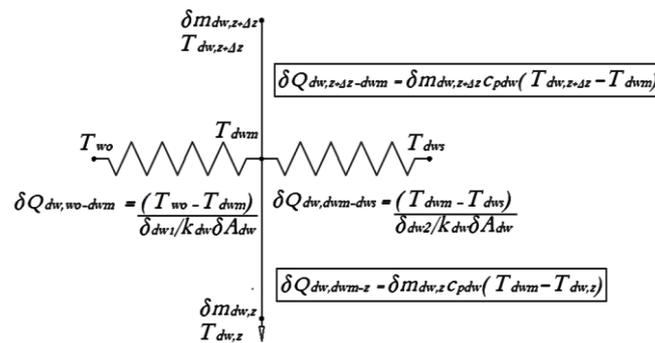
Figure 9: Deluge water-side thermal resistance diagram

c) The heat transfer balance for the thermal resistance diagram

$$\delta Q_{dw,wo-dwm} + \delta Q_{dw,z+\Delta z-dwm} = \delta Q_{dw,dwm-dws} + \delta Q_{dw,dwm-z} \tag{29}$$

d) Coupling of the elementary control volume to thermal resistance diagram

$$\delta Q_{dw,wo-dwm} = \delta Q_{dw,y_3} = \delta Q_{w,y_3} \tag{30}$$

$$\delta Q_{dw,dwm-dws} = \delta Q_{dw,y_4} \tag{31}$$

From the momentum balance of the elementary control volume within the deluge water film, the deluge water film thickness and the deluge water weighted mean temperature respectively were defined as

$$\delta_{dw,z} = \left(\frac{3\mu_{dw}\delta m_{dw,z}}{\rho_{dw}g\Delta x(\rho_{dw} - \rho_a)}\right)^{\frac{1}{3}} = \delta_{dw1} + \delta_{dw2} \tag{32}$$

$$T_{dwm} = T_{wo} - \frac{5(T_{wo} - T_{dws})}{8} \tag{33}$$

2.1.5.　Air-side elementary control volume
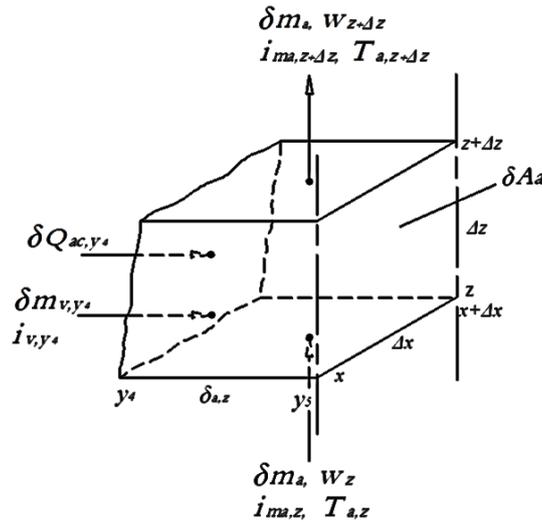
Figure 10: Air-side elementary control volume

a)　　The water mass balance for the elementary control volume

$$\delta m_{v,y_4} + \delta m_a(1 + w_z) = \delta m_a(1 + w_{z+\Delta z}) \tag{34}$$

Substitute Eq. (26) into Eq. (34) and simplify so that

$$\delta m_{v,y_4} = \Delta \delta m_{dw,z} = \delta m_a \Delta w_z \tag{35}$$

b)　　The energy balance for the elementary control volume

$$\delta Q_{ac,y_4} + \delta m_{v,y_4} i_{v,y_4} + \delta m_a i_{ma,z} = \delta m_a i_{ma,z+\Delta z} \tag{36}$$

Substitute Eq. (35) into Eq. (36) and simplify

$$\delta Q_{ac,y_4} + \delta m_a \Delta w_z i_{v,y_4} = \delta m_a \Delta i_{ma,z} \tag{37}$$
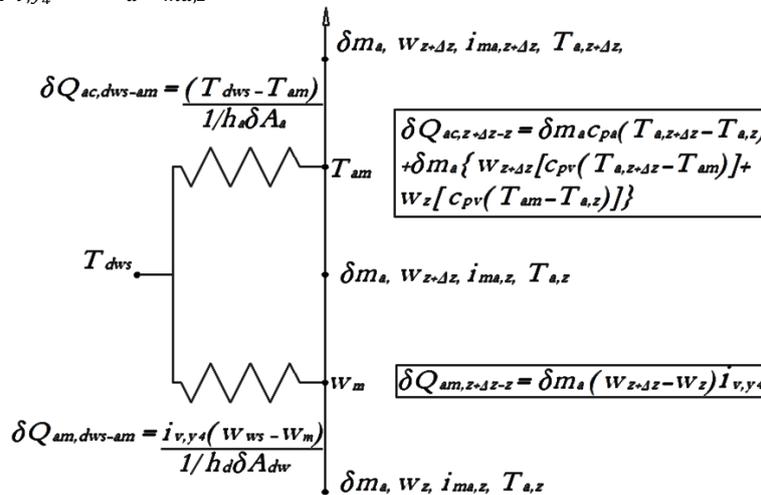
Figure 11: Air-side thermal resistance diagram

c)　　The heat transfer balance for the thermal resistance diagram

$$\delta Q_{ac,dws-am} = h_a \delta A_a (T_{dws} - T_{am})$$
$$= \delta m_a c_{pa}(T_{a,z+\Delta z} - T_{a,z}) + \delta m_a w_{z+\Delta z} c_{pv}(T_{a,z+\Delta z} - T_{am}) \tag{38}$$
$$+ \delta m_a w_z c_{pv}(T_{am} - T_{a,z})$$

$$\delta Q_{am,dws-am} = h_d \delta A_{dw} i_{v,y_4}(w_{sw} - w_m) = \delta m_a i_{v,y_4}(w_{z+\Delta z} - w_z) \tag{39}$$

d)　　Coupling of the elementary control volume to thermal resistance diagram

$$\delta Q_{am,dws-am} = \delta Q_{am,z+\Delta z-z} = \delta m_{v,y_4} i_{v,y_4} \tag{40}$$

$$\delta Q_{ac,dws-am} = \delta Q_{ac,z+\Delta z-z} = \delta Q_{ac,y_4} \tag{41}$$

2.1.6.   The governing equations

In order to obtain the governing equations, describing the processes taking place in each elementary control volume, as well as in the entire two-dimensional elementary control volume, the differential equations derived in sections 2.1.1, 2.1.2, 2.1.3, 2.1.4, and 2.1.5 were coupled and simplified.

In addition to those equations, other differential equations were found to be:

$$\delta_{c1} = \frac{(T_{cs} - T_{cm})\delta_c}{(T_{cs} - T_{wi})} \tag{42}$$

$$\delta_{c2} = \frac{(T_{cm} - T_{wi})\delta_c}{(T_{cs} - T_{wi})} \tag{43}$$

$$\Delta\delta m_{c,z} = \frac{k_c \delta A_i (T_{cs} - T_{cm})}{\delta_{c1} i_{s,x}} = \frac{k_c \delta A_i (T_{cs} - T_{wi})}{\delta_c i_{s,x}} \tag{44}$$

$$\delta_c = \left[\frac{8k_c \mu_c (T_{cs} - T_{wi})z}{\rho_c g (\rho_c - \rho_v) i_{s,x}}\right]^{1/4} = \delta_{c1} + \delta_{c2} \tag{45}$$

where $i_{s,x}$ is the steam enthalpy, and it is determined as

$$i_{s,x} = i_{fg,x} + c_{pv}T_v \tag{46}$$

$$\delta_{dw1} = \frac{(T_{wo} - T_{dwm})\delta_{dw}}{(T_{wo} - T_{dws})} \tag{47}$$

$$\delta_{dw2} = \frac{(T_{dwm} - T_{dws})\delta_{dw}}{(T_{wo} - T_{dws})} \tag{48}$$

2.2.   Discretization of the governing equations

In order to derive the governing equations for the numerical model, the governing differential equations were discretised into simple and solvable algebraic equations. The tube bundle was divided into several control volumes/ grids in the z-direction as depicted in Figure 12. The discretised governing equations were achieved by employing the linear upwind differencing scheme. The linear upwind differencing scheme is mainly used in the convection dominated flows, because it provides the numerical stable solutions and takes into account the flow direction[19].
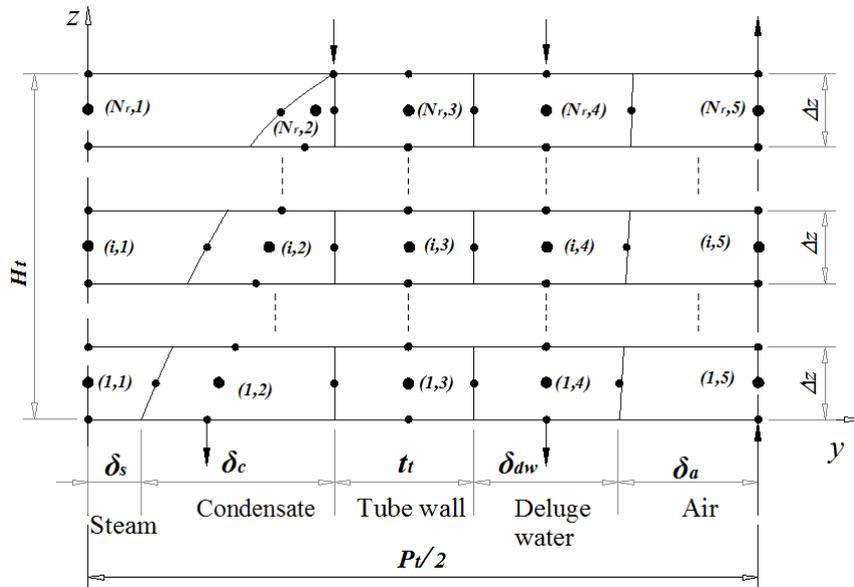
Figure 12: Grid points network

The first number or subscript i of the indices notation used in Figure 12 denotes the grid point index in the z-direction, and the second number or subscript j denotes the grid point index in the y-direction. The height of each grid cell was determined as

$$\Delta z = H_t/N_r \tag{49}$$

where, H_t is tube height and N_r is the number of intervals/rows in the z-direction.

To show the generally application of the linear upwind differencing scheme, the nodal grid point P at the centre of the cell (i, j) was considered. The neighbouring cells of point P were denoted as N, S, W and E, and the interface grid points between them and point P are designated as n, s, w and e, as illustrated in Figure 13.
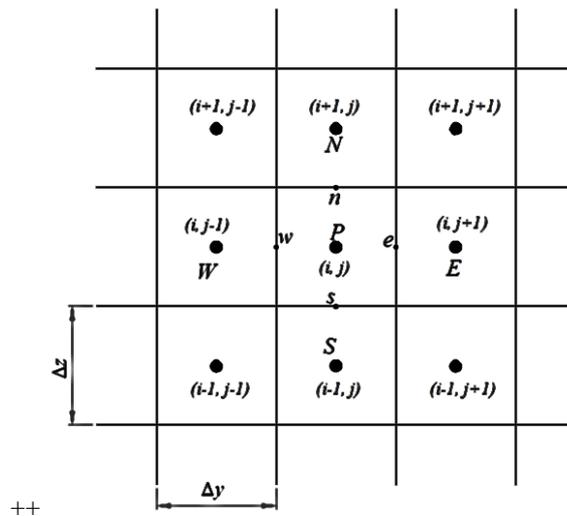
Figure 13: General discretization using linear upwind differencing scheme

The derivatives of a considered property (ϕ) at nodal point P in the z-direction can be expressed as

$$\frac{d\phi}{dz}\Big|_{P(i,j)} = \frac{\phi_{n(i,j)} - \phi_{s(i,j)}}{\Delta z} \tag{50}$$

where $\phi_{n(i,j)}$ and $\phi_{s(i,j)}$ are values of property (ϕ) at the interface grid points n and s, respectively.

$$\phi_{n(i,j)} = \frac{\phi_{P(i,j)} + \phi_{N(i,j)}}{2} = \frac{\phi_{(i,j)} + \phi_{(i+1,j)}}{2} \tag{51}$$

$$\phi_{s(i,j)} = \phi_{P(i,j)} + \frac{\phi_{P(i,j)} - \phi_{N(i,j)}}{2} = \phi_{(i,j)} + \frac{\phi_{(i,j)} - \phi_{(i+1,j)}}{2} \tag{52}$$

2.3.   Solution methods

For the comprehensive assessment of thermal performance of the tube bundle, a two-dimensional analysis was conducted by employing heat and mass transfer analogy method of analysis. The discretised governing equations of a two-dimensional model were solved numerically. The numerical method is complex and consumes time. However, it is analogous to the laboratory experiment and provides a set of solutions that indicate the distribution of the variables within the domain[20].

For each control volume the local temperature value at grid point as well as the local heat transfer across the control volume was determined. The evaluation and calculations are performed interval by interval starting from the top of the tube bundle.

Procedure of solving method:

1) The boundary initial values of condensate temperature and mass flow rate, tube wall temperature, deluge water inlet temperature, outlet air temperature and humidity ratio for the top grid cells were assumed. The steam condensation was assumed to take place at constant condensing temperature.
2) The calculations were performed for the whole top interval, until all the discretised governing equations were satisfied.
3) The input values of the top interval were then taken as the output values of the interval below.
   This procedure was repeated for each interval until the given boundary conditions at the bottom of the tube bundle were satisfied.

2.4.   Grid dependency of numerical solutions

The accuracy of the numerical solutions is sensitive to grid cell sizes. Therefore, the solution grid dependency was conducted to ensure that the numerical solutions were grid independent. The manual grid refinement method was employed to investigate the impacts of the grid dependency on the numerical solutions. In order to attain the grid independent numerical results, the tube bundle was divided into several intervals/rows (N_r) in the z-direction. As the number of the intervals increases, the size of the grid cells become smaller and the variations in the numerical solutions become lesser, and therefore solutions tend toward constant values.

The flow on the air-side was considered based on Figure 14. The critical tube height (H_{cr}) at which two air-side boundary layers reach the symmetric line between the tubes, as shown in Figure 14, was computed. The flow within the critical height was considered to be a developing flow, and therefore the heat transfer rate and air-side pressure drop within this region were determined by employing the external flow theories. The flow in the rest of the air flow channel (δ_a) was considered to be a fully developed flow.
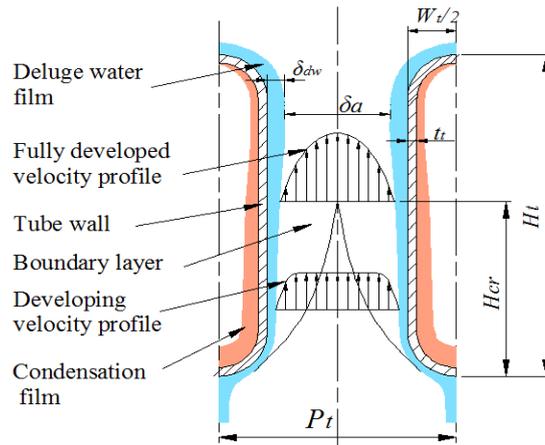
Figure 14: Tube bundle section, illustrating the air-side flow between two adjacent tubes[2]

The effect of the physical grid cells' size on the numerical solutions is shown in Figure 15. The normalised values of calculated variables, as presented in the legends of the graph, are plotted against the number of intervals. From Figure 15, it is clear that up to interval number 15, ($N_r = 15$), the numerical results highly vary with grid cells' size; while beyond interval number 15, the variations in the numerical solutions are slight smaller and the solutions can be taken as constant. Therefore, the solutions are grid independent as from interval number 15, and that further grid refinement will provide grid independent solutions.
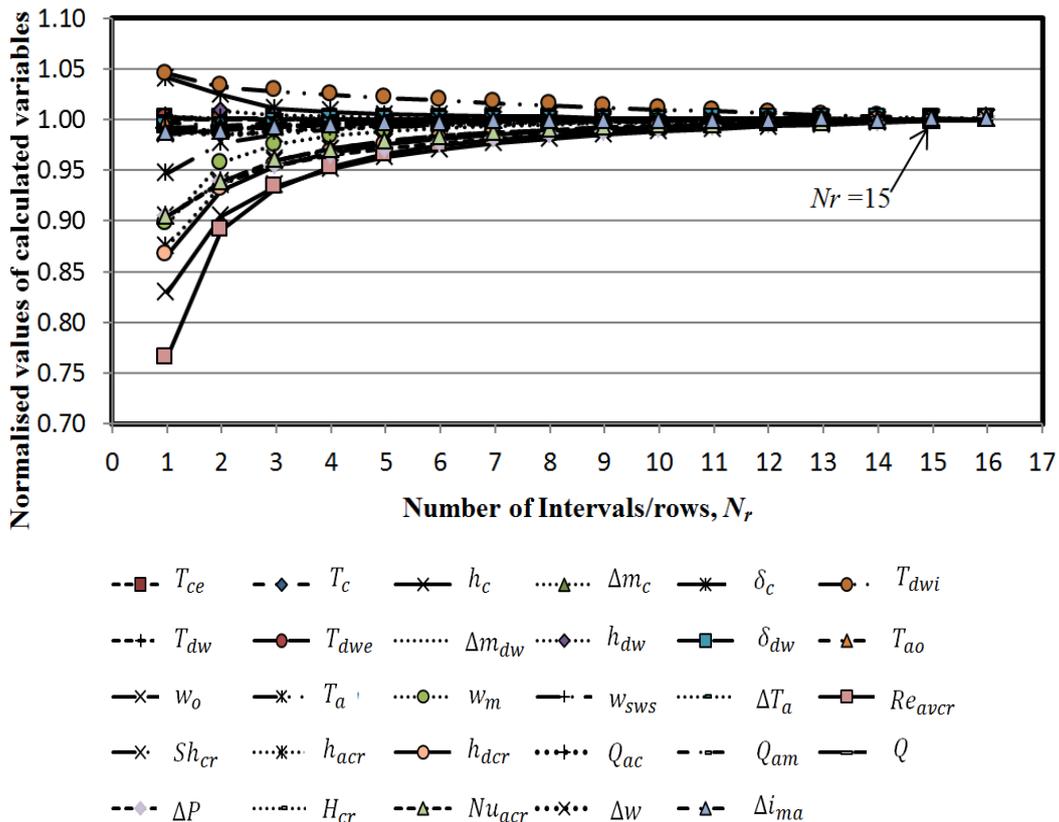
Figure 15: Graph illustrating the grid dependency of the numerical solutions

2.5.   *Validation of a two-dimensional numerical model*

The validation of numerical two-dimensional model was carried out in order to find out whether the two-dimensional method was adequate to provide the correct results, for predicting the bundle's performance. This was performed by comparing the numerical two-dimensional solutions to the one-dimensional solutions presented in Angula[2].Solutions obtained from one and two-dimensional methods were comparable. However,

there was a slight discrepancy in the heat transfer rate with differences of 1.98%, 8.23%, and 10.79% obtained from the heat and mass analogy, Merkel and Poppe methods respectively. The discrepancies between one and two-dimensional solutions were mainly attributed to the assumptions of constant temperature difference between steam and deluge water or air made in one-dimensional model and variation of air and water properties in two-dimensional model. The difference in air-side pressure drop yielded from all methods was found to be insignificant. Therefore, the two-dimensional model was demonstrated to be valid for the analysis of the thermal performance of a delugeable flat bare tube air-cooled steam condenser bundle.

2.6. Performance analysis

The configuration of a delugeable flat tube bundle that yielded higher performance was identified by comparing its performance to that of round tube bundle presented in Anderson[15]. During the comparisonstudy, the effects of the tube pitch, tube height, and the steam flow area on the heat transfer rate ratio (Q_r/Q_f) and air-side pressure drop ratio $(\Delta P_r/\Delta P_f)$ of the delugeable round and flat bundles were investigated. The frontal area and fan power were kept constant at the value that equal to that of the round tube bundle. Furthermore, the same deluge water mass flow rate as was considered for the round tube bundle was employed. The best configuration of a delugeable flat tube bundle was found to be the one that provides a higher rate of heat transfer at a reasonable air-side pressure drop. The round tube bundle considered by Anderson[15], is depicted in Figure 16, and the performance data of this tube bundle are shown in Table 2.

Tube layout
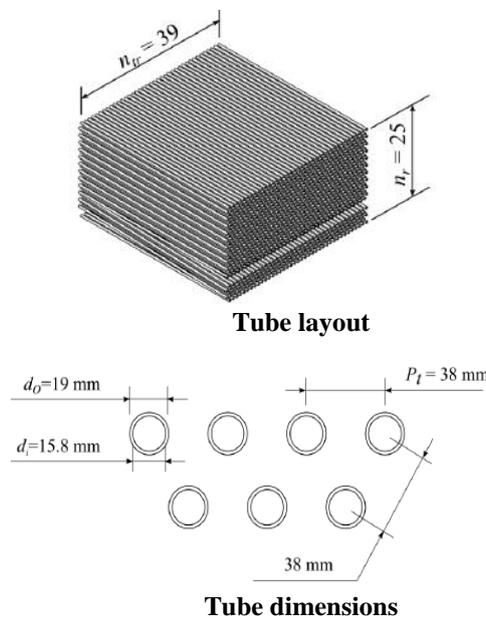
Tube dimensions
Figure 16: Tube bundle presented by Anderson [15]

Table 2: The performance data of a round tube bundle presented by Anderson[15]

Description	Symbol	Units	Operating mode	
			wet	dry
Heat transfer rate	Q	MW	5.126	0.627
Air-side pressure drop	ΔP	P_a	22.703	22.50
Fan power	P_F	W	417.98	417.892

The investigation of the tube pitch and tube height on the performance ratio of the bundles, was carried out in the same way as it was conducted in Angula[2]. For the assessment of tube pitch impacts on the performance ratio of the bundles, four tube pitches of 23; 25; 30 and 35 mm were considered. For each tube pitch, the performance ratio was analysed for three different steam flow areas of $A_{sf1} = 0.368$ m^2, $A_{sf2} = 2A_{sf1}$ and $A_{sf3} = 2A_{sf1}$; whereby the first steam flow area is equal to the round tube bundle's steam flow area. The tube width corresponding to each steam flow area was computed. This investigation was conducted for both wet and dry operating modes, and the tubes' height was kept constant at 1 m. The number of the tubes per row computed for each considered pitch is shown in Table 3.

Table 3: Number of tubes per row for the flat tube bundle configurations

Description	Symbol	Unit				
Tube pitch	P_t	mm	23	25	30	35
Number of tubes per row	n_{tr}		125	115	96	82

The effect of the tube height on the performance ratio of the bundles was examined for three tube heights of 0.5; 1; and 1.2 m. The tube pitch of 30 mm was considered in this investigation, despite a low performance obtained at this pitch compared to the performance yielded at the tube pitch of 23 and 25 mm. The investigation of the tube height effects at small tube pitches was found to become impossible and unrealistic for short tubes as the steam flow area changes from A_{sf2} to A_{sf3}.

III. RESULTS AND DISCUSSION

3.1. Influence of tube pitch on the performance ratio of the bundles

The heat transfer rate ratios (Q_r/Q_f) and air-side pressure drop ratios ($\Delta P_r/\Delta P_f$) of the round and flat tube bundle are illustrated in Figure 17 and 18 respectively. For a constant tube pitch, slight variations in the attained results for different tube widths were noticed. However, significant differences in the results was observed at various tube pitches. This indicates that the tube pitch has a substantial effect on the bundle's performance than the tube width. Moreover, the tubes with small width were found to perform better than those with large widths at small tube pitches. While, the wider tubes were found to perform better at the large tube pitches. This is due to the fact that for large tube pitches, the air-side pressure drop between the tubes is low. Therefore, since the fan power was constant, the air velocity between tubes was increased in order to achieve the targeted fan power. As the tube pitch and tube width increase, the air-side pressure drop ratio was found to increase and drop respectively.
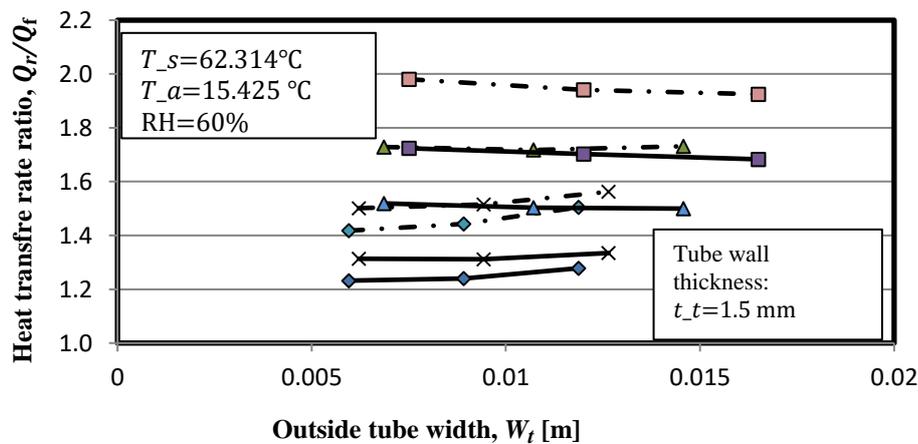
Figure 17: Effect of the tube pitch on the heat transfer rate ratio of round and flat tube bundle
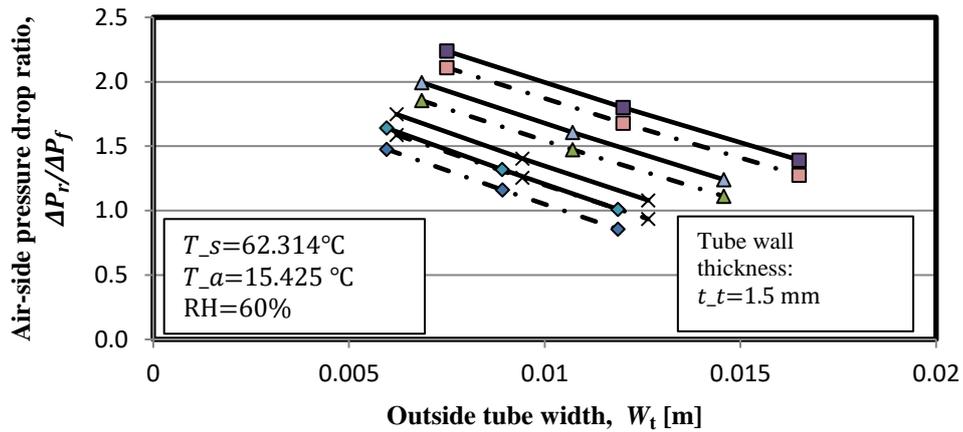
Figure 18: Effect of the tube pitch on the air-side pressure drop ratio of round and flat tube bundle

- P_t = 23 mm, wet
- P_t = 25 mm, wet
- P_t = 30 mm, wet
- P_t = 23 mm, dry
- P_t = 25 mm, dry
- P_t = 30 mm, dry
- P_t = 35 mm, wet
- P_t = 35 mm, dry

3.2. *Influence of tube height on the performance ratio of the bundles*

The yielded heat transfer rate (Q_r/Q_f) and air-side pressure drop ($\Delta P_r/\Delta P_f$) ratios of a round and flat tube bundle are displayed in Figure 19 and 20. The short tube height was found to have significant negative impact in the bundle performance especially for the large tube width. This is due to the fact that for the constant steam flow area, the tube becomes wider when its height decreases.
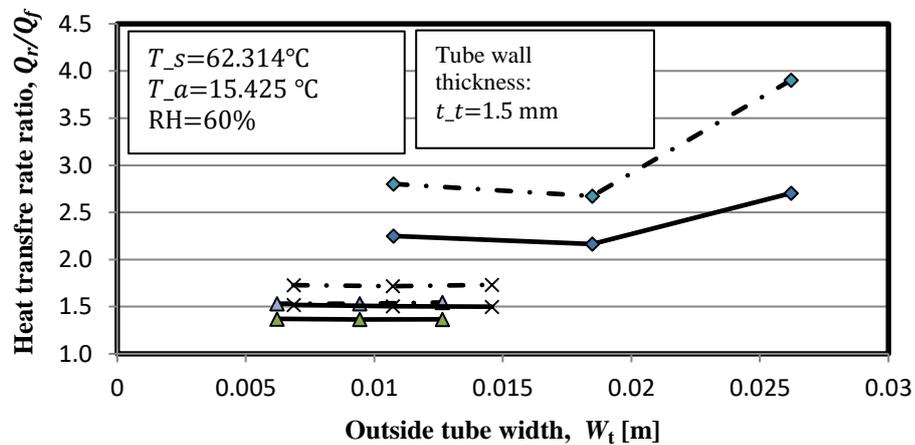
Figure 19: Effect of the tube height on the heat transfer rate ratio of round and flat tube bundle
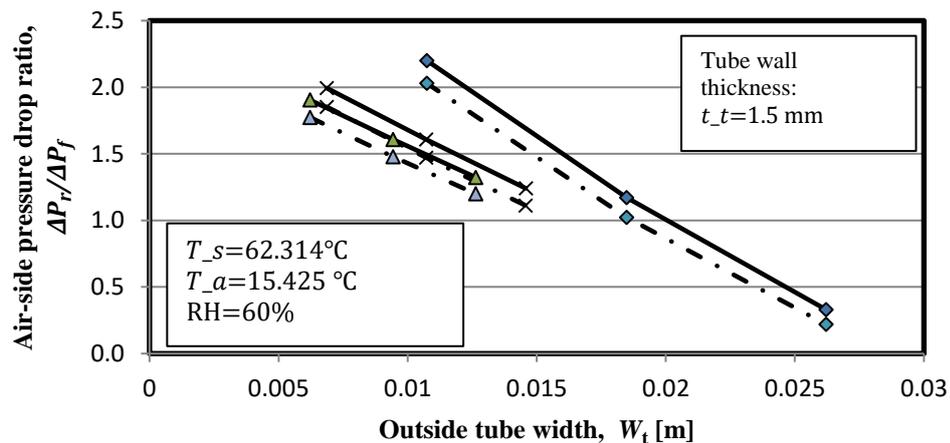
Figure 20: Effect of the tube height on the air-side pressure drop ratio of round and flat tube bundle

– ◆ – H_t = 0.5 m, wet   – × – H_t = 1 m, wet   – ▲ – H_t = 1.2 m, wet

—◆— H_t = 0.5 m, dry   —×— H_t = 1 m, dry   —▲— H_t = 1.2 m, dry
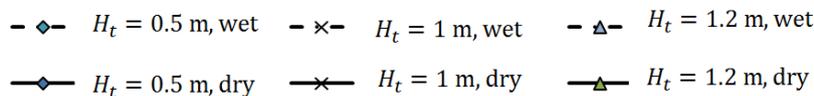
From the data presented above, the small tube pitches were found to deliver high performance than large pitches. However, their performance analyses were found to become unrealistic and impossible at some points, as the steam flow area increases. Therefore, the best bundle configuration was found to consist of tubes of 1 m long, with 3.86 and 6.86 mm inside and outside width respectively, and arranged with a tube pitch of 30 mm. Furthermore, the round tube bundle performance was better than that of the flat tube bundle. In comparison with the selected flat tube bundle configuration, the performance of the round tube bundle was found to be around 1.95 times, and 1.43 times, when both bundles operate as an evaporative and dry air-cooled condenser respectively. These results correlate very well with the results of one-dimensional analysis presented in Angula[2].

IV. CONCLUSIONS

In this paper, a two-dimensional model employed in the analysis of the thermal performance of the deluged flat tube bundle of a second stage of an induced draft HDWD of an ACSC was developed. A two-dimensional model was presented by a set of discretised governing differential equations, and it was validated by comparing its results to one-dimensional solutions. This model was used to configured the best flat tube bundle configuration, by comparing its performance to the round tube bundle performance.

REFERENCES

[1].   J. A. Heyns and D. G. Kröger, "Performance Characteristics of an Air-Cooled Steam Condenser with a Hybrid Dephlegmator," *R & D Journal of the South African Institution of Mechanical Engineering,* vol. 28, pp. 31-36, 2012.
[2].   E. Angula, "Modelling of a delugeable flat bare tube bundle for an air-cooled steam condenser," *International Journal of Science And Engineering,* vol. 4, no. 4, 2018.
[3].   R. O. Parker and R. E. Treybal , "The heat, mass transfer characteristics of evaporative coolers," *AIChE Chem Eng Progr Symp Ser 57,* vol. 32, p. 138–149, 1961.
[4].   T. Mizushina, R. Ito and H. Miyashita, "Experimental study of an evaporative cooler," *International Chemical Engineering,* pp. 727-732, 1967.
[5].   F. Merkel, "Verdunstungskuling," *VDI-Zeitschrift,* vol. 70, pp. 123-128, 1926.
[6].   A. Hasan and K. Siren , "Performance investigation of plain and finned tube evaporatively cooled heat exchangers," *Applied Thermal Engineering,* vol. 23, p. 325–340, 2003.
[7].   W. J. Yang and D. W. Clark , "Spray cooling of the air-cooled compact heat exchangers," *International Journal of Heat and Mass Transfer,* vol. 18, pp. 311-317, 1975.
[8].   W. Leidenforst and B. Korenic , "Evaporative Cooling and Heat Transfer Augmentation Related to Reduced Condenser Temperatures," *Heat Transfer Engineering,* vol. 3, pp. 38-59, 1982.
[9].   K. A. Jahangeer, A. O. Andrew, M. Tay and I. Raisul , "Numerical investigation of transfer coefficients of an evaporatively-cooled condenser," *Applied Thermal Engineering,* vol. 31, pp. 1655-1663, 2011.
[10].   F. Zhang , J. Bock, A. M. Jacobi and H. Wu, "Simultaneous heat and mass transfer to air from a compact heat exchanger with water spray precooling and surface deluge cooling," *Applied Thermal Engineering ,* vol. 63, pp. 258-540, 2014.
[11].   A. Hasan and K. Siren , "Performance investigation of plain circular and oval tube evaporatively cooled heat exchangers," *Applied Thermal Engineering,* vol. 24, p. 777–790, 2004.

[12]. W. Y. Zheng , Z. Dong-Sheng , S. Jin , Z. Li-Ding and Z. Hong-jian , "Experimental and computational analysis of thermal performance of the oval tube closed wet cooling tower," *Applied Thermal Engineering,* vol. 35, pp. 233-239, 2012.

[13]. J. A. Heyns , "Performance characteristics of an air-cooled steam condenser incorporating a hybrid (dry/wet) dephlegmator," *Master Thesis, University of Stellenbosch, RSA,* 2008.

[14]. Owen, "Air-cooled condenser steam flow distribution and related dephlegmator design considerations," *Doctor Thesis, Stellenbosch University, RSA,* 2013.

[15]. N. R. Andreson, "Evaluation of the performance characteristics of a hybrid (dry/wet) induced draft dephlegmator," *Master Thesis, University of Stellenbosch, RSA,* 2014.

[16]. H. Graaff, "Performance Evaluation of a Hybrid (dry/wet) Cooling System," Master of Engineering (Mechanical),, Stellenbosch University, RSA, 2017.

[17]. H. Reuter and N. Anderson, "Performance evaluation of a bare tube air-cooled heat exchanger bundle in wet and dry mode," *Applied Thermal Engineering,* 2016.

[18]. M. Poppe and H. Rögener, "Evaporative Cooling Systems," *VDI-Warmeatlas, Section Mh,* 1984.

[19]. H. K. Verseteeg and M. Malalasekera, An introduction to computational fluid dynamics. The fnite volume Method, second edition, London: Ashford Colour Press, 2007.

[20]. V. P. Suhas, Numerical heat transfer and fluid flow, Series in computational methods in mechanics and thermal sciences, Washington, D.C. : Hemisphere, 1980.

NOMENCLATURE

A	Area	m^2	**Subscripts**		
c_p	Specific heat at constant pressure	[J/kg K]	a	Air	
			v	vapour	
d	Diameter of duct	[m]	ac	Convection heat transfer	
g	Gravitation acceleration	[m/s^2]	am	Mass transfer	
H	Height	[m]	cr	Critical	
h	Heat transfer coefficient	[W/m K]	c	Condensate	
			cm	Condensate mean	
h_d	Mass transfer coefficient	[kg/m^2 s]	cs	Condensate surface	
			$c1$	Between condensate surface and mean	
i	Enthalpy	[J/kg]	$c2$	Between condensate mean and tube wall	
i_{fg}	Latent heat	[J/kg]	dw	deluge water	
k	Thermal conductivity	[W/mK]	dwm	Deluge water mean	
L	Length	[m]	dws	Deluge water surface	
m	Mass flow rate	[kg/s]	$dw1$	Between tube wall and deluge water mean	
NTU	Number of transfer units		$dw2$	Between deluge water mean and surface	
N,n	Number		f	Flat	
P	Pitch	[m]	g	Gravity	
Q	Heat transfer rate	[W]	i,j	Grind point index	
RH	Relative humidity	[%]	m	mean	
t	Thickness	[m]	N,S,W,E	Grid cells	
T	Temperature	[°C]	n,s,w,e	Interface grid points	
U	Overall heat transfer coefficient	[W/m^{2}K]	o	outlet	
			r	Rows or intervals or round	
W	Width	[m]	s	Surface or steam	
w	Humidity ratio	[kg /kg]	sf	Steam flow	
x	Co-ordinate or distance	[m]	sw	Saturated water	
y	Co-ordinate or distance	[m]	t	Tube	
y_1,y_2,y_3,y_4, y_5	Distance	[m]	tr	Tube row	
			$y_1,y_2,y_3,y_4 y_5$	Location or position	
z	Co-ordinate or distance	[m]			
Dimensionless groups					
Le_f	Lewis factor, $h_a/c_{pam}h_d$				
NTU	Number of transfer units				